Journal of Magnetism and Magnetic Materials 508 (2020) 166729

Contents lists available at ScienceDirect

Journal of Magnetism and Magnetic Materials

journal homepage: www.elsevier.com/locate/jmmm

Research articles

Spin-resolved electron transport in nanoscale heterojunctions. Theory and applications

Artur Useinov[a,*], Hsiu-Hau Lin[b], Niazbeck Useinov[c], Lenar Tagirov[d,e]

[a] International College of Semiconductor Technology, National Chiao Tung University, Hsinchu 30010, Taiwan
[b] Department of Physics, National Tsing Hua University, Hsinchu 30013, Taiwan
[c] Institute of Physics, Kazan Federal University, Kazan 420008, Russia
[d] Zavoisky Physical-Technical Institute, FRC Kazan Scientific Center of RAS, Kazan 420029, Russia
[e] Tatarstan Academy of Sciences, Institute of Applied Research, Kazan 420111, Russia

ARTICLE INFO

Keywords:
Spintronics
Interconnects
Heterojunctions
Point contact
Ballistic magnetoresistance
Spin-resolved conductance
Spin-resolved contact resistance
Domain wall resistance
Tunnel magnetoresistance

ABSTRACT

The work represents the extended theoretical model of the electrical conductance in nanoscale magnetic point-like contacts. The developed approach describes diffusive, quasi-ballistic, ballistic and quantum regimes of the spin-resolved conductance that is important for further development of the contact Andreev reflection spectroscopy, heterojunction models, scanning tunnel microscopy techniques. As a benefit, the model provides a unified description of the contact resistance from Maxwell diffusive through the ballistic to purely quantum transport regimes without residual terms. The model of the point contact assumes that the contact area can be replaced by a complicated object (*i.e.* the tunnel barrier or complicated one with nanoparticles, narrow domain wall, *etc.*), where the potential energy profile determines its electrical properties. The model can be easily adapted to particular contact materials, its physical properties and species of the contact area.

1. Introduction

Quantitative theory of conductance G in various electronic systems with restricted geometry has numerous important applications, *e.g.*, in a case of point contacts it solves the problem of determining the size of the contact [1–3]. The conductivity of point contacts (PCs) has been studied during many years in the past [4]. At present time, great efforts have been made to create reliable PCs or nanocontacts (NCs) with predictable properties, considering the interface matching of the nanowire connections between normal, semiconductor, ferromagnetic (FM) and superconducting materials in nanoscale spintronics devices [5–11].

A simplest, but relevant in most cases, solvable model for the PC is a circular constriction of the radius a, which connects two large electron reservoirs. It is convenient to quantify the conducting properties of the NC *via* the dimensionless ratio of the geometrical size a to the bulk electron mean free path l. The a/l or it's inverse, the Knudsen ratio $K = l/a$, becomes an output of a fitting of the theory to experimental data on the resistance of the PCs [12]. Once l is known from resistivity measurements of the material, the effective diameter of the contact can be estimated from the fitted K.

The model diameter $d = 2a$ can be identified as the size of the contact, if information about the contact shape is unavailable. Two limiting regimes of the conductance through NCs are commonly discussed. The first one is the Maxwell, or diffusive conductance G_M, when the contact size much larger than l ($K \ll 1.0$) [13–15],

$$G_M = 2a/\rho_V, \tag{1}$$

where ρ_V is the bulk resistivity, which can be expressed in terms of bulk conductivity σ_V of the isotropic metal as follows:

$$\rho_V^{-1} = \sigma_V = \frac{e^2 n\, l}{\hbar k_F} = \frac{e^2 p_F^2 l}{3\pi^2\hbar^3}, \tag{2}$$

where e, $k_F = p_F/\hbar$ and $n = k_F^3/3\pi^2$are the electron charge, Fermi wave-number and free electron density in metals, respectively. Within the model, the bulk mean free path $l = \hbar k_F \tau/m_e$ (m_e is the electron mass) depends on impurities concentration, defects, electron-electron and electron-phonon scattering *via* the average time τ between collisions.

The second regime refers to the ballistic conductance through the contact area when no any collisions occur during the electron transmission [16], $K \gg 1.0$. In this case, there is no place or information about l in the Sharvin conductance:

* Corresponding author.
E-mail address: artu@nctu.edu.tw (A. Useinov).

https://doi.org/10.1016/j.jmmm.2020.166729
Received 26 February 2019; Received in revised form 27 February 2020; Accepted 9 March 2020
Available online 12 March 2020

$$G_S = \frac{e^2 a^2 k_F^2}{4\pi\hbar} = G_0 N. \tag{3}$$

The factor $G_0 = 2e^2/h = 7.7481\cdot 10^{-5}\Omega^{-1}$ is the conductance quantum, $N \simeq (k_F a/2)^2$ is the number of open conductance channels accommodating the nanoconstriction [7,17].

Furthermore, it is relatively easy to obtain the expressions, which show the connection between G_S, σ_V and G_M: $G_S = \frac{3\pi a}{4K}\sigma_V$, $\sigma_V = \frac{4K}{3\pi a}G_S$ and $G_M = \frac{8K}{3\pi}G_S$. It is noticed that Sharvin [16] estimated asymptotic behavior of the resistance as $R_S \simeq p_F/e^2(2a)^2 n$. An expression of Sharvin conductance in the form of $G_S = 3\pi/(16R_S)$ with accuracy up to $3\pi/16$ factor is used in literature [2,18,19]. In general case, n is a complicated function of k_F. Hence, if the system is not limited by the model of free electrons, the n might be corrected according properties of the specified material and its Fermi surface, so n and k_F can be determined within *ab initio* calculations as well.

Moreover, there is another view of the Sharvin conductance, which is often used [2,18,19]:

$$G_S = \frac{3\pi a^2}{4\rho_V l}. \tag{4}$$

It is obtained by multiplying the numerator and denominator of (3) by l and applying (2). Expression (4) has an advantage in the case of constriction (*i.e.* a contact of identical metals), it can be applied for estimating the effective constriction radius a. Indeed, according to Eq. (2), the product $\rho_V l$ = constant is independent of l. Provided that the product $\rho_V l$ is known, ρ_V can be obtained from resistivity measurements, and l can be extracted *via* the size effects in thin films and nanowires (NWs), or combining the resistivity with specific heat measurements and utilizing the Pippard relations [20,21]. It seems that Eq. (4) represents a useful tool to estimate the NC size.

The problem can be considered from the opposite point of view: once the contact size is known in some way, the resistance measurements give a tool to estimate $\rho_V l$ - product, *i.e.* establish the contact material parameter from the single kind of measurements. Indeed, it has been done for Au-Au nanocontacts [18], where it was pointed out that the procedure to extract l from $\rho_V l$ = constant has yielded $l = 3.8$ nm, which is an order of magnitude below the bulk $l \simeq 38$ nm for 99.99% pure gold [22] at room temperature. Moreover, it was noticed that the range of applicability of the ballistic Sharvin approach, (3) or (4), is restricted to a smallest radius of the contacts close to 1 nm, otherwise, the accordance of the theory with the relevant experiment is poor. Thus, both diffusive Maxwell and ballistic Sharvin limits of the NC conductance cover extreme limits keeping unexplored a wide gap of most accessible and relevant sizes from 1 nm to 100 nm.

The analysis of the electron transport through a circular constriction at arbitrary relationship between the orifice radius a and the mean free path l has been made by Wexler [12]. It is based on the variation solution for the Green function (GF) of the Boltzmann kinetic equations. The obtained solution for the resistance was represented as follows [12]:

$$R_W = \frac{1}{G_W} = \frac{1}{G_M}\gamma(K) + \frac{1}{G_S}, \tag{5}$$

where G_W is defined as the Wexler conductance, $\gamma(K)$ is a slowly varying function with the asymmetric values $\gamma(K \to 0) = 1.0$, and $\gamma(K \to \infty) = 9\pi^2/128 = 0.694$. Expression (5) has the form of an interpolation formula combining additively the diffusive Maxwell and ballistic Sharvin resistances, the relevant terms are vanishingly small when one of them approaches the related limit. The gamma factor gives a smooth transition from one regime to the other by inclining the asymptotics to the correct values.

In 1999 Nikolic and Allen [23] reconsidered the Wexler solution for the orifice conduction for the non-magnetic junctions. The stationary Boltzmann and Poisson equations for the electric potential were solved taking into account the Bloch-wave propagation and Fermi-Dirac statistics in presence of an electric field. It is worthy to note, that this solution is referred to in literature as the most accurate solution [24] (see, however, strong assumptions after Eq. (59) in Ref. [23] when formulating an easy-to-use outcome of the approach. The low-order solution was cast into the form of the Wexler solution with a proper $\gamma(K)$ re-definition, Fig. 2 in Ref. [23]). At the same time, Mikrajuddin *et al.* [25] proposed the approach of the resistance model, which is based on the solution of the electrostatic Laplace problem, summing up the resistances of the infinitesimal shells between equipotential surfaces in the orifice constriction. The result is represented in the form of Eq. (5) with the re-defined $\gamma(K)$. The comparison of the Nikolic-Allen and Mikrajuddin *et al.* solutions shows the significant difference between them, which again refreshes the interest to the problem. To summarize, the theoretical approach of the orifice constriction, which is determined *via* the classical electrodynamics, results in the sum of the diffusive and ballistic terms with a complex transition between them.

We propose an alternative approach, which is based on the quasiclassical transport formalism [26–28]. The outcome and advantage of our solution is a simple integral expression, which provides smooth functional transition between the Sharvin and Maxwell limits without residual terms or counterparts. Moreover, this result is derived as a limiting case from a general quantum model of the NC, where NC can be built from different magnetic metals or metal alloys. As example of verification, the theoretical model is applied to explain experimental data for the golden NCs (symmetric, non-magnetic limit of the general theory) as well as to explain the resistance impact of the single domain wall (DW) in magnetic NWs.

2. Theoretical model of the spin-resolved electron transport in heterojunction

In this section, the model of the NC is considered in terms of the extended quasiclassical approach, which is based on solution of the transport differential equations for the quasiclassical GFs. The model is formulated as a boundary problem in which two large electron reservoirs (leads) are linked *via* the general NC's interface, Supplementary Material. The NC itself can be a simple constriction or a complicated structure containing e.g. a tunnel barrier. It is important only that the internal NC's structure could be solved quantum-mechanically, and then the electric current through the NC is expressed in terms of the boundary solution, solving the problem of the conduction. The application of this method is suitable for the heterostructure dimensions larger than the Fermi wavelength of a free electron, $\lambda_F = 2\pi/k_F$ which is approximately 0.5 nm.

Considering the general case of FM hetero-contact, which is composed of different FM metals, we assume that the spin-dependent Fermi wave-numbers in both sides of the contact $k_{F,\alpha}$ as well as l_α ($\alpha = \uparrow, \downarrow$) are accounted as arbitrary parameters. The NC is modeled by a conductive circular orifice of the radius a obtained in an impenetrable membrane. This membrane divides the space into the left (L) and right (R) half-spaces, and each half-space is assigned to a single magnetic domain, Fig. 1. The geometry of this NC matches with the cylindrical coordinate system $[\mathbf{r}, \phi, z]$, where z is the symmetry axis. The voltage V, which is applied far away from the contact area by equipotential planes, induces the electrical current $I^z = I^z_\downarrow + I^z_\uparrow$. The solution for the net charge current I^z_α with the spin projection α and positive bias, which is applied to the right terminal, can be brought to the form:

$$I^z_\alpha = \frac{e^2(k_{\min})^2 a^2 V}{2\pi\hbar}\int_0^\infty dk \frac{J_1^2(ka)}{k} F_\alpha(k), \tag{6}$$

where k is the wave-number conjugated to the radial variable in the contact plane; $k_{\min}$ is minimum one of the two wave-numbers: $k^L_{F,\alpha}$ and $k^R_{F,\alpha}$; $J_1(ka)$ is the Bessel function, appearing after the integration over the contact plane, the detailed derivation is given in the Supplementary Material. Despite the external similarity of expression (6) with those given earlier in our works [28–30], the integrand function $F_\alpha(k)$ is

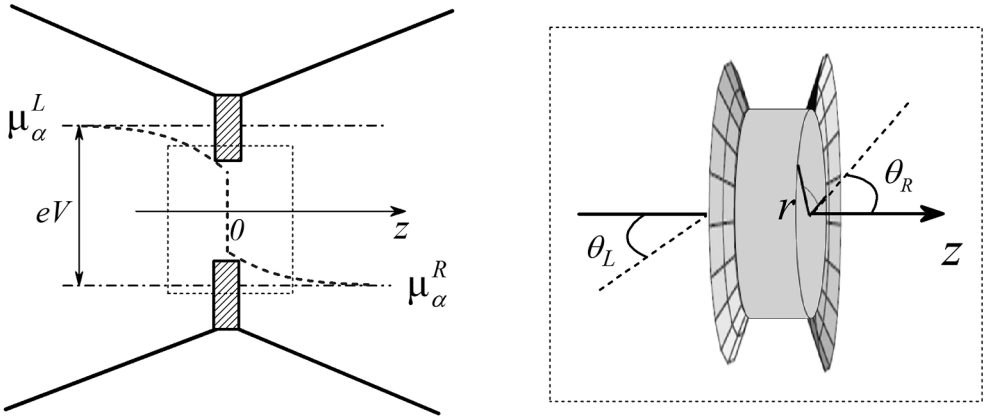

Fig. 1. The schematic view of NC with chemical potential drop. The selected rectangular area shows the contact interface in a non-conductive membrane. In general case, an electron with $k^L_{F,\alpha}$ and trajectory angle $\theta_{L,\alpha}$ transmits through the NC to the right-hand side having outgoing parameters $k^R_{F,\alpha}$ and $\theta_{R,\alpha}$, respectively.

completely reconsidered:

$$F_\alpha(k) = \langle x_L D_\alpha\rangle_{\theta_L} - (N_1\langle x_L W_L\rangle_{\theta_L} + N_2\langle x_L W_R\rangle_{\theta_L}), \tag{7}$$

where D_α is the quantum-mechanical transmission coefficient; $x_L = \cos(\theta_L)$; The angle between the z-axis and direction of the electron trajectory is $\theta_{c,\alpha}$, which is related to the contact side $c = L(R)$, see Fig. 1. The averaging over solid angle is given in spherical coordinate system $[\mathbf{k}, \theta, \varphi]$, and $\langle\ldots\rangle_{\theta_L}$ is equivalent to $\frac{1}{2\pi}\int_0^{2\pi} d\varphi \int_0^{\theta_{cr}} \sin(\theta_L)(\ldots)d\theta_L = \int_{\tilde{x}}^1 (\ldots)dx_L$, where the limit $\tilde{x} = \cos(\theta_{cr})$ appears as a result of the electron momentum conservation along the direction of the contact's plane. The index α is hidden, but refers to all variables throughout. Further quantities are displayed as follows:

$$N_1 = \{\langle D_\alpha\rangle_{\theta_L}[2(1-\lambda_R)+\lambda_2] - \langle D_\alpha\rangle_{\theta_R}\lambda_4\}\Delta^{-1},$$

$$N_2 = \{\langle D_\alpha\rangle_{\theta_R}[2(1-\lambda_L)+\lambda_1] - \langle D_\alpha\rangle_{\theta_L}\lambda_3\}\Delta^{-1},$$

$$\Delta = 4(1-\lambda_L)(1-\lambda_R) + 2[\lambda_1(1-\lambda_R) + \lambda_2(1-\lambda_L)] - \lambda_3\lambda_4 + \lambda_1\lambda_2,$$

where

$$\lambda_{L(R)} = \frac{1}{1+k^2 l^2_{L(R)}}$$

$$\lambda_1 = \left\langle \frac{D_\alpha}{(1+(kl_L)^2(1-x_L^2))^{3/2}} \right\rangle_{\theta_L}$$

$$\lambda_2 = \left\langle \frac{\delta\cdot x_L D_\alpha}{\sqrt{x_L^2+x_{cr}^2}\,(1+(kl_R\delta)^2(1-x_L^2))^{3/2}} \right\rangle_{\theta_L}$$

$$\lambda_3 = \left\langle \frac{\delta\cdot x_L D_\alpha}{\sqrt{x_L^2+x_{cr}^2}\,(1+(kl_L)^2(1-x_L^2))^{3/2}} \right\rangle_{\theta_L}$$

$$\lambda_4 = \left\langle \frac{D_\alpha}{(1+(kl_R\delta)^2(1-x_L^2))^{3/2}} \right\rangle_{\theta_L}$$

$$\langle x_L W_L\rangle_{\theta_L} = \left\langle \frac{x_L D_\alpha}{(1+(kl_L)^2(1-x_L^2))^{3/2}} \right\rangle_{\theta_L}$$

$$\langle x_L W_R\rangle_{\theta_L} = \left\langle \frac{x_L D_\alpha}{(1+(kl_R\delta)^2(1-x_L^2))^{3/2}} \right\rangle_{\theta_L}.$$

The expressions above include $\langle D_\alpha\rangle_{\theta_R} = \left\langle \frac{\delta\cdot x_L D_\alpha}{\sqrt{x_L^2+x_{cr}^2}} \right\rangle_{\theta_L}$ and $\delta = k^L_{F,\alpha}/k^R_\alpha(V)$, where the spin index α is conserved for the wave vector $k^R_\alpha(V) = \sqrt{(k^R_{F\alpha})^2 + (2m_R e/\hbar^2)V}$ according the assumption that the spin diffusion length is larger than the contact dimension. The lower integral limit becomes $\tilde{x} = 0$ $(\theta_{cr} = \pi/2)$ at the condition $\delta \leqslant 1$, otherwise $\tilde{x} = \sqrt{(\delta^2-1)/\delta^2}$, or both conditions can be joined as follows: $\tilde{x} = \mathrm{Re}[\sqrt{(\delta^2-1)/\delta^2}]$. The solution for the reversed bias V with negative terminal on the right-hand side can be retrieved using the symmetry of the system: $k^L_{F,\alpha} \to k^R_\alpha(V)$, $k^R_\alpha(V) \to k^L_{F,\alpha}$ that gives again the positive terminal on the right side. It is assumed that the left side is grounded and the conduction band edge does not move with V, the Fermi level is fixed, otherwise: $k^R_\alpha(V) = \sqrt{(k^R_{F\alpha})^2 + (2m_R e/\hbar^2)V/2}$ and $k^L_\alpha(V) = \sqrt{(k^L_{F\alpha})^2 - (2m_L e/\hbar^2)V/2}$, and $\delta = k^L_\alpha(V)/k^R_\alpha(V)$.

The transmission coefficient D_α is a function of the applied voltage V and parameters of the potential energy profile within NC area. It should be noticed that transmission D_α for 2D and 3D electron transport, which is characterized originally by 1D potential energy profile $U(z)$, becomes a function of $\theta_{c,\alpha}$ and V, consisting the projections of the Fermi wave-vectors on the z-axis: $k^{\perp L}_\alpha = k^L_{F\alpha}\cos(\theta_{L,\alpha})$ and $k^{\perp R}_\alpha = k^R_\alpha(V)\cos(\theta_{R,\alpha})$. It should be noticed, that the derived set of the variables, such as λ_c, $\lambda_{1..4}$, $\langle x_L W_c\rangle_{\theta_c}$ as a functions of k in (6) and (7), is significantly different from the set in our previous works [28–30], while the ballistic and tunnel-responsible term $\langle x_L D_\alpha\rangle_{\theta_L}$ is conserved. The origin of this difference is the accurate solution of the integro-differential equation which takes into account the second-order derivatives of the GFs by z. The mathematical derivation of Eq. (6) is collected in Supplementary Material.

The general solution (6) can be verified applying it to the case of symmetric non-magnetic contact: $D_{\uparrow,\downarrow} = 1.0$, $l_{L,R} = l$, $k^L_F = k^R_F = k_F$, and thus $F_\downarrow(k) = F_\uparrow(k)$, $I^z_\uparrow = I^z_\downarrow$. The replacement of the variable $y = ka$ in Eq. (6) results to $\int_0^\infty dy\, J_1^2(y)/y = 1/2$. For the infinitesimal applied voltage V the conductance $G = \frac{dI}{dV} = (I^z_\uparrow + I^z_\downarrow)/V$ reads:

$$G = 4G_S\left(\frac{1}{4} - \int_0^\infty \frac{dy}{y}\frac{J_1^2(y)}{1+y^2K^2+\sqrt{1+y^2K^2}}\right), \tag{8}$$

which satisfies the exact Maxwell and Sharvin limits automatically. It is an advantage of the revisited derivation of the present work against the previous ones [28–30]. One might expect that it gives also more precise $I-V$ curves for the non-magnetic NCs. The analytical solution Eqs. (6)–(8) is applied in the next section for the comparison with alternative theoretical approaches and fitting the experimental data available in literature.

3. Discussion: applicability of the model

The general approach, that we developed in the present work, covers a variety of the NC realizations, which might be involved further in the development of the quantum integrated circuits for the next generation of electronics below 10 nm. Potentially, the model can deal

with spin-resolved conducting properties of the nanoscale elements such as interconnects, complicated magnetic tunnel junctions (MTJs), quantum dots, spin field-effect transistors (FETs), *etc*. As a first-order approximation, the contact area can be replaced by a simple or composite quantum object, where the electric properties are determined by the internal structure of the energy levels and/or the potential energy profile across the junction. For instance, the spin-resolved quantum term $F_\alpha = \langle x_L D_\alpha \rangle_{\vartheta_L}$ of the model was successfully applied for the simple MTJs [31–33] as well as for MTJs with embedded nanoparticles [34,35] explaining the voltage dependence of the tunnel magnetoresistance TMR(V), the quantized conductance behavior [34] and $R(V)$ curves. The improved model Eqs. (6)–(8) extends further the range of applicability, making it more adequate to the real systems.

3.1. The orifice conductance: comparison with alternative theoretical models

One of the goals of this work is to compute the classical conductance for the non-magnetic junction and compare it with that obtained in the earlier theories. The proposed approach allows to reproduce the Maxwell and Sharvin analytical limits in such terms that they smoothly transform from one to the other exactly without some additional factors like γ in Refs. [12,23,25]. Indeed, at $K \to \infty$ ($a/l \to 0$) the integral in Eq. (8) vanishes, hence, the conductance transforms into the ballistic Sharvin one, $G = G_S$. The integral in Eq. (8), at small $K \ll 1$ ($a/l \gg 1$), reads $\left(\frac{1}{4} - \frac{2K}{3\pi}\right)$ that gives accurate solution for the diffusive limit, $G = (8/3\pi)KG_S = G_M$. In contrast to the Wexler and the followers' solutions, in which the ballistic term is always a part of (5) for any K, our solution (8) exactly transforms from the ballistic to the diffusive limit of the conductance.

The normalized conductance by the Sharvin limit is given in Fig. 2a for the four solutions of the problem, the result of the present work is shown as $R_1 = G/G_S$. The ratios $R_2 = \widetilde{G}/G_S$, $R_3 = G_{W'}/G_S$ and $R_4 = G_W/G_S$ correspond to the solutions by Mikrajuddin *et al.* with $\gamma \approx \frac{2}{\pi}\int_0^\infty e^{-K\cdot x}\mathrm{sinc}(x)\,dx$, by Nikolic and Allen with $\gamma_{\mathrm{fit}} \approx (1 + 0.83K)/(1 + 1.33K)$ and, finally, by the Wexler approach with flexible γ, respectively. The comparison of the relative differences of the conductance to R_1, which is displayed in Fig. 2b, shows that the Mikrajuddin solution is the closest one to our result. The Nikolic-Allen solution $G_{W'}$ with relevant γ_{fit} shows the maximal difference of 15.8% with ours at $a/l \approx 1$. It should be noticed, the presented $G_{W'}$ is the lowest order solution with a maximal deviation of 1.0% against the most exact summed-up series solution in [23]. The Wexler solution shows the intermediate deviation of 12.9% at $a/l \approx 0.75$. We believe that the strong assumption created by Wexler [Ref. [12], the paragraph after Eq. (42)], where the numerical coefficient 9/8 is replaced by 1 at the Knudsen-Sharvin limit, and the one which is made by Nikolic and Allen [Ref. [23], the paragraph after Eq. (59)], where the numerical coefficient 3/4 is also replaced by 1 at the same limit, could be a cause of the deviations in the vicinity of the Sharvin limit reported above.

Finally, it should be noticed that some experimental works manipulate with γ in Eq. (5), in order to achieve the desired fitting, considering $\gamma \approx 0.7$–0.75 as a reduced constant, *e.g.* [2,18,19]. We assume that their reduced value of γ originates from the striving to compensate the inaccuracy of the Wexler model for the quasi-ballistic region $a/l \approx 0.25 - 4.0$, Fig. 2b, nevertheless that it can give a valuable deviation from a real value for l, being estimated at the larger scales, *e.g.* for $a/l \approx 10$.

3.2. Conductance of the golden nanocontacts

The experimental data by Erts *et al.* [18] is considered for a quantitative comparison with our theory. The conductance for the golden NCs was measured with different dimensions and fitted by Wexler's model finally resulting in $l \simeq 3.8\,\mathrm{nm}$ [18]. The drastic reduction of l in the NCs was attributed to a high density of scattering centers, which are created during the point contact formation process.

Considering the golden contacts in the ballistic conductance regime, we found that the experimental points from Ref. [18] lie predominantly between the straight lines of the Sharvin conductance at $k_F^{\mathrm{Au}} = 0.8\,\mathrm{Å}^{-1}$ and $k_F^{\mathrm{Au}} = 0.9\,\mathrm{Å}^{-1}$, Fig. 3a. The Fermi wave-number in the bulk for the gold can be estimated using the electron density $n = 5.9 \times 10^{22}\ \mathrm{cm}^{-3}$, and thus $k_F^{\mathrm{Au}} = (3\pi^2 n)^{1/3} = 1.205\,\mathrm{Å}^{-1}$ [Ref. [36], Chapter 1, Table 1.1], the value corresponds to the line 5 for G in a contrast with lines 1-4 in Fig. 3a.

It makes sense to go beyond a ballistic conductance regime in analysis of the experimental data of Erts *et al.* [18], because most probably, they refer to the quasi-ballistic regime of the conductance (see Fig. 2). Fig. 3b shows theoretical curves of the contact conductance derived from (8), where the $k_F^{\mathrm{Au}}$and l values were considered as independent parameters. The fitted curves 1 – 4 refer to $k_F^{\mathrm{Au}} = 1.1\,\mathrm{Å}^{-1}$, $k_F^{\mathrm{Au}} = 1.0\,\mathrm{Å}^{-1}$, $k_F^{\mathrm{Au}} = 0.9\,\mathrm{Å}^{-1}$ and $k_F^{\mathrm{Au}} = 0.85\,\mathrm{Å}^{-1}$ with $l = 4.0\,\mathrm{nm}$, $l = 6.0\,\mathrm{nm}$, $l = 10.0\,\mathrm{nm}$ and $l = 38.0\,\mathrm{nm}$, respectively. Utilizing (2) in the form $n = k_F^{\mathrm{Au}}/(\pi\, l\, G_0 \rho_V^{\mathrm{Au}})$, where $\rho_V^{\mathrm{Au}} = 22.14\,\Omega{\cdot}\mathrm{nm}$, the related parameters correspond to $n = 5.1 \times 10^{23}\,\mathrm{cm}^{-3}$, $n = 3.09 \times 10^{23}\,\mathrm{cm}^{-3}$, $n = 1.67 \times 10^{23}\,\mathrm{cm}^{-3}$ and $n = 4.15 \times 10^{22}\,\mathrm{cm}^{-3}$ for the curves 1 – 4, respectively. It seems that the experimental points lie predominantly on the curve 4. Moreover, the curve 4 has the closest value by n, which is estimated in Ref. [36].

The experimental data, which cover not only quasi-ballistic but also the diffusive regimes of the conductance as well, might be determinative to verify our theoretical model. Fortunately, experiments of Jensen *et al.* [37] with golden NCs extend further the measurement range,

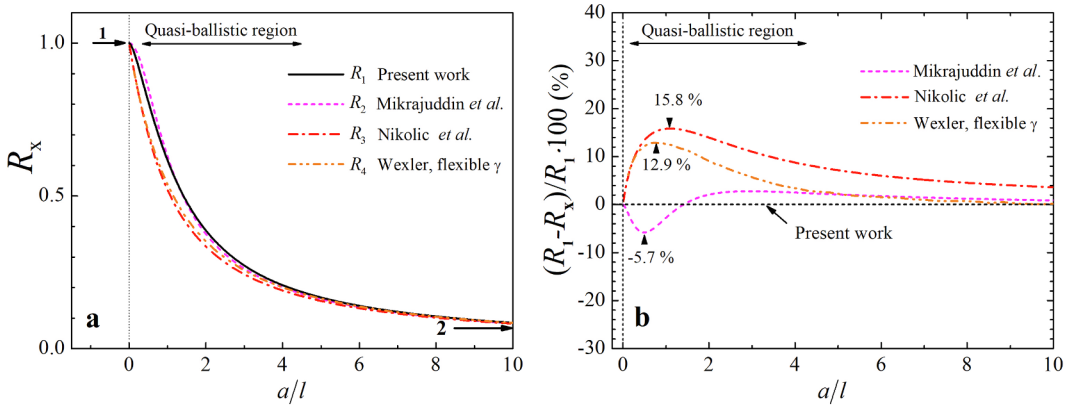

Fig. 2. (a) The conductance ratios R_x of the different models, where $R_1 = G/G_S$, $R_2 = \widetilde{G}/G_S$, $R_3 = G_{W'}/G_S$ and $R_4 = G_W/G_S$ correspond to the models of the present work, Mikrajuddin, Nikolic-Allen and Wexler approach with flexible γ, respectively. The arrows 1 and 2 point to the ballistic and diffusive limits, respectively. (b) The relative difference for the relevant ratios in respect to R_1.

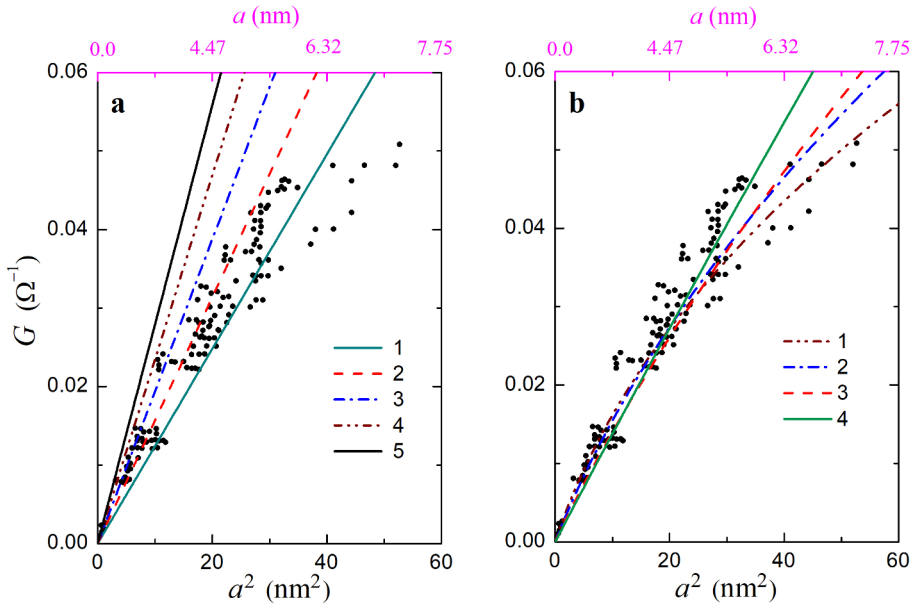

Fig. 3. The conductance of the golden NCs with various contact dimensions. (a) Theoretical curves 1–5, ascribed to the ballistic regime at $k_F^{Au} = 0.8$ Å^{-1}, $k_F^{Au} = 0.9$ Å^{-1}, $k_F^{Au} = 1.0$ Å^{-1}, $k_F^{Au} = 1.1$ Å^{-1} and $k_F^{Au} = 1.2$ Å^{-1}, respectively. (b) Curves 1–4 correspond to $k_F^{Au} = 1.1$ Å^{-1}, $k_F^{Au} = 1.0$ Å^{-1}, $k_F^{Au} = 0.9$ Å^{-1}, and $k_F^{Au} = 0.85$ Å^{-1} with $l = 4.0$ nm, $l = 6.0$ nm, $l = 10.0$ nm and $l = 38.0$ nm, respectively. The black dots refer to the experimental data [18].

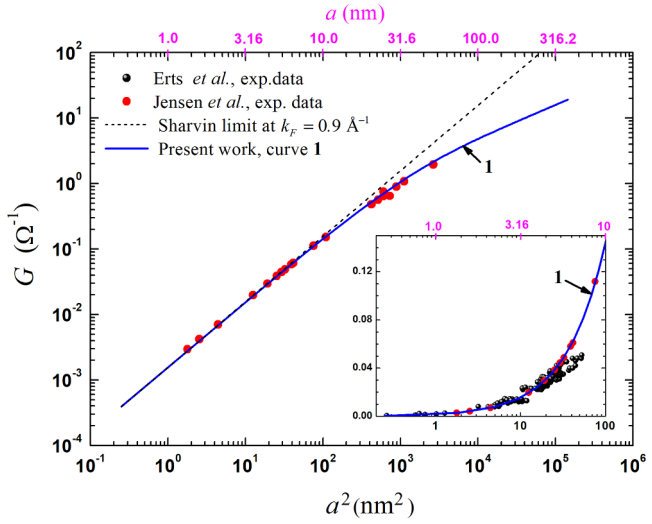

Fig. 4. The conductance of the golden NCs with the various contact radius. The red circles are the data adapted from Fig. 4 in Ref. [37]. The ballistic limit is estimated at $k_F^{Au} = 0.9$ Å^{-1}, while the curve 1 is obtained from Eq. (8) with $k_F^{Au} = 0.9$ Å^{-1} and $l = 38$ nm.

which was partly covered by Erts *et al.*, towards the diffusive regime of the conductance. Fig. 4 shows the best fit of our model Eq. (8) to the Jensen data. The theory matches the experimental data almost ideally with the fitting parameters $k_F^{Au} = 0.9$ Å^{-1} and $l = 38$ nm. Both datasets by Erts and Jensen are collected in the inset of Fig. 4 together, keeping the linear scale for G.

The remaining discrepancies in k_F^{Au} values with respect to the textbook references, as well as the large scatter in the estimated l, which may satisfactorily describe the existing experimental data, should not raise doubts about the correctness of the approach: the lateral shape deviation from the ideal circular orifice and the opening angle of the constriction might also influence the conductance quantitatively, giving a correction up to ~50% [38].

3.3. Domain wall resistance in magnetic nanowires

We apply the developed model to calculate the conductance of a magnetic NW with and without single DW. It demonstrates the full range of the spin-resolved ballistic and diffusive electron transport regimes, that is suited to explain a DW resistance behavior, for example, in $Ni_{80}Fe_{20}$ Permalloy (Py) [39], Co/Ni [40,41] and Co NWs [42]. Since a difference in resistance of NWs with and without DW is a subject of our interest, only DW contribution $\Delta R = (R_{DW} + R_{NW}) - (R_0 + R_{NW})$ is calculated for a wide range of diameters, Fig. 5a. Thus, the resistance of the homogeneous wire's segments, $R_{NW} = 4\rho_V l_{NW}/\pi d^2$, cancels in the difference, where l_{NW} is total length of NW. The other terms $R_{DW(0)} \simeq V/(I_{\uparrow}^{DW(0)} + I_{\downarrow}^{DW(0)})$ are resistances of a DW or an interface between segments of the composite NW. The spin-dependent currents $I_{\uparrow,\downarrow}^{DW(0)}$ are estimated within the general magnetic case of the heterojunction Eq. (6) with low bias approach, when the integral distribution is voltage-independent. A spin-bands transition has been taken into account for the case with DW (R_{DW}), while the case without DW assumes $D_{\uparrow,\downarrow} = 1.0$ for R_0 in the case of homogeneous NW. The assignment of spin sub-bands with respect to the quantization axis is opposite in the case of the opposite direction of the domain's magnetizations, Fig. 5b. The vortex states and the area between them in [39] are simplified to 1D DW representation in our case similarly to Ref. [40,41]. The DW impact is integrated into the present model in the same way as in Ref. [29], where D_α for the DW is considered as an exact analytical solution for the sloping potential profile between two spin-split conduction bands. The values of the spin-dependent density of states (DOS) at the Fermi level are taken proportional to $k_{F,\alpha}$. The spin diffusion length, the length of the spin conservation, is assumed to be much larger than the fixed DW width (d_{DW}).

The model estimations are compared with experimental data of the resistance difference ΔR in Py [39], Co/Ni [40] and Co nanowires [42], which are shown as symbols in Fig. 5a. The first experimental point $\Delta R \approx 0.3\,\Omega$ is shown as magenta triangle for Py NW with $d = 350$ nm [Ref. [39], Fig. 4a] that corresponds to the case $l_{\uparrow}/l_{\downarrow} \approx 4.5$. The second experimental point (green diamond) with $\Delta R \approx 1.2\,\Omega$ referes to Co/Ni NW with $d = 80$ nm [Ref. [40], Fig. 2b and c]. Red square points correspond to $\Delta R \approx 2.178\,\Omega$ and $\Delta R \approx 7.5\,\Omega$ for Co NW with $d = 50$ nm and $d = 35$ nm, respectively [Ref. [42], Fig. 1]. The black dashed line, which is drawn for $l_{\uparrow}/l_{\downarrow} = 4$, fits well the experimental points except for the

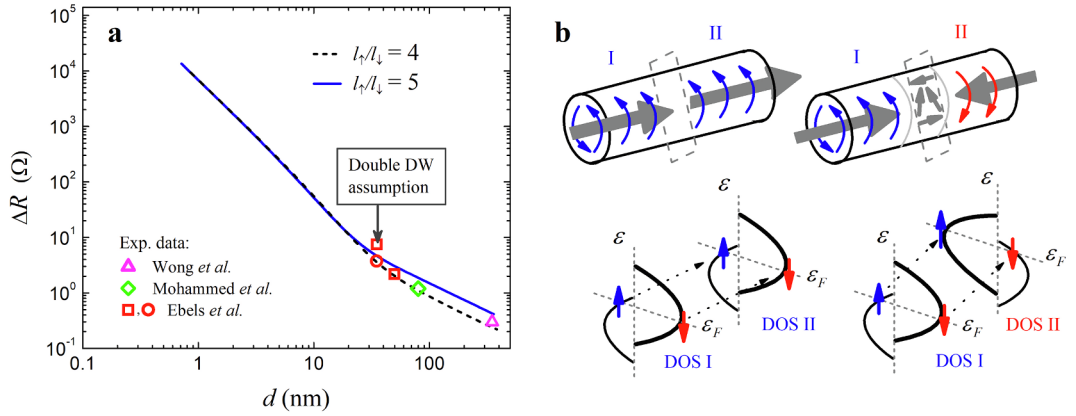

Fig. 5. (a) Individual impact of the DW resistance in NW *versus* its diameter d. The model parameters for the dashed black curve are $l_\downarrow = 3.0$ nm, $l_\uparrow = 12.0$ nm, and for the solid blue line: $l_\downarrow = 2.5$ nm, $l_\uparrow = 12.5$ nm; Both curves calculated at $k_{F\downarrow}^{L(R)} = 1.08$ Å^{-1}, $k_{F\uparrow}^{L(R)} = 0.61$ Å^{-1}, $d_{\mathrm{DW}} = 3.0$ nm. Experimental points by Wong, Mohammed and Ebels *et al.* correspond to Py, Co/Ni and Co NWs with single DW, respectively. (b) The sketch of the two vortex magnetic states and electron transitions with the DOS differences: without (left) and with DW (right). The vortex magnetic states are shown similar to that in the experimental paper [39] and marked as the color thin arrows, while the theoretical DW representation is simplified to 1D case and magnetization is shown as the large gray arrows.

case of Co NW with $d = 35$ nm. Following the assumption that this point corresponds to the case of two DWs connected in series, the additional red circle is depicted as half of the ΔR for $d = 35$ nm as a reduction to the case of single DW. It should be noticed, Ebels *et al.* [42] has also considered the assumption of the presence of two DWs for $d = 35$ nm.

In general, it is found that ΔR rapidly reduces with increasing of d, however, the curve's slope decreases when the conductance transforms from quasi-ballistic to a diffusive regime for the spin-up conductance channel at $d \approx 2l_\uparrow$. The curve for ΔR is sensitive to the mean free path ratios. Experimental measurements of the spin-split l_α are accessed in [43,44], theoretical estimations are available in Ref. [22]. The considered k_F-values are also consistent with the literature data: $k_{F\uparrow\downarrow}^{\mathrm{Py}}$ are similar to Mu-metal (Py-type) compounds [29]. It should be noticed also that, taking into account the spin-flip effect and spin accumulation might further improve the consistency of the material parameters utilized in the data fittings.

4. Conclusions

In the present work, a quasi-classical transport model is developed as an approach for computing of electron transport through the point-like contact. The spin-resolved quantum, ballistic, quasi-ballistic and diffusive regimes of the transport are covered by the theory. The solution includes the boundary conditions in terms of the quantum-mechanical transmission coefficient for the NC interface. The NC interface potentially can be replaced by any quantum object, where the transmission coefficient can be spin-resolved, depending on the applied voltage, the strength of the magnetic field or any other external parameter affecting the energy profile properties. As a result, the analytical solution is derived for the general spin-resolved case for the system, obeying cylindrical symmetry. It doesn't require so much computer programming to represent it in the form, which allows to make the comparison and fitting to the experiment. The theory has great generality: it can handle with spin-resolved conduction of the nano-scale objects such as NCs, single and multi-barrier tunnel junctions, MTJs with embedded nanoparticles, allowing in some cases to see the quantized conductance, *etc*.

Finally, we applied our general expression for the current through the NC to a particular problem of the conductance between two separated metallic (nonmagnetic) leads, which are connected by a short and small orifice and filled with the same metal. The simple expression for the conductance that we have got from our general solution provides the smooth functional transition between the Sharvin ballistic and Maxwell-Holm diffusive limits without residual terms. The theory fits quite well the existing experimental data for the golden NCs. Another application is also shown, which concerns the DW resistance in ferromagnetic nanowires. The comparison to the existing experimental data shows a reasonable quantitative agreement, confirming the wide range of applicability.

Author Contribution

A.U. and L.T. developed a theoretical approach. A.U. wrote the detailed analytical solution in supplementary materials and performed numerical simulations, he was responsible for a programming and data visualization; A.U. and L.T. discussed and wrote the manuscript, while N.U. and H.H.L. made an additional independent validation and formal analysis; L.T. provided the data curation and methodology of the article.

Declaration of Competing Interest

The authors declare that they have no known competing financial interests or personal relationships that could have appeared to influence the work reported in this paper.

Acknowledgment

This work is dedicated to the blessed memory of late Prof. Peter Grünberg and Dr. Boris Vodopyanov. It was financially supported by Ministry of Science and Technology (MOST) Taiwan (Grant No. MOST-107-2218-E-009-024-MY3, MOST-108-3017-F-009-003), and by the "Center for the Semiconductor Technology Research" from The Featured Areas Research Center Program within the framework of the Higher Education Sprout Project by the Ministry of Education (MOE) in Taiwan. N.U. acknowledges the Program of Competitive Growth of Kazan Federal University for the partial support. L.T. acknowledges funding by the state assignment No. AAAA-A18-118030690040-8 *via* FRC Kazan Scientific Center of RAS.

Appendix A. Supplementary data

Supplementary data associated with this article can be found, in the online version, at https://doi.org/10.1016/j.jmmm.2020.166729.

References

[1] N. García, M. Muñoz, Y.W. Zhao, Magnetoresistance in excess of 200% in ballistic Ni nanocontacts at room temperature and 100 Oe, Phys. Rev. Lett. 82 (1999) 2923–2926.

[2] R.S. Timsit, Electrical conduction through small contact spots, Proceedings of the 50th IEEE Holm conference on electrical contacts and the 22nd international

conference on electrical contacts, 2004, pp. 184–191, https://doi.org/10.1109/HOLM.2004.1353116.
[3] Y.G. Naidyuk, I.K. Yanson, Point-contact spectroscopy, Springer-Verlag, New York, 2005, https://doi.org/10.1007/978-1-4757-6205-1.
[4] A.G.M. Jansen, A.P. van Gelder, P. Wyder, Point-contact spectroscopy in metals, J. Phys. C: Solid State Phys. 13 (1980) 6073–6118.
[5] R.J. Soulen, J.M. Byers, M.S. Osofsky, B. Nadgorny, T. Ambrose, S.F. Cheng, P.R. Broussard, C.T. Tanaka, J. Nowak, J.S. Moodera, A. Barry, J.M.D. Coey, Measuring the spin polarization of a metal with a superconducting point contact, Science 282 (1998) 85–88.
[6] G. Deutscher, Andreev-Saint-James reflections: a probe of cuprate superconductors, Rev. Mod. Phys. 77 (2005) 109–135.
[7] G.B. Lesovik, I.A. Sadovskyy, Scattering matrix approach to the description of quantum electron transport, Phys. Usp 54 (2011) 1007–1059.
[8] E. Tartaglini, T.G.A. Verhagen, F. Galli, M.L. Trouwborst, R. Müller, T. Shiota, J. Aarts, J.M. van Ruitenbeek, New directions in point-contact spectroscopy based on scanning tunneling microscopy techniques (Review Article), Low Temp. Phys. 39 (2013) 189–198.
[9] T.M. Klapwijk, S.A. Ryabchun, Direct observation of ballistic Andreev reflection, J. Exp. Theor. Phys. 119 (2014) 997–1017.
[10] W.-C. Lee, W.K. Park, H.Z. Arham, L.H. Greene, P. Phillips, Theory of point contact spectroscopy in correlated materials, Proc. Nat. Acad. Sci. 112 (2015) 651–656.
[11] W.-C. Lee, L.H. Greene, Recent progress of probing correlated electron states by point contact spectroscopy, Rep. Prog. Phys. 79 (2016) 094502.
[12] G. Wexler, The size effect and the non-local Boltzmann transport equation in orifice and disk geometry, Proc. Phys. Soc. 89 (1966) 927–941.
[13] J.C. Maxwell, A Treatise on Electricity and Magnetism, unabridged 3rd ed., Dover Publications, New York, 1954.
[14] R. Holm, Electric Contacts, unabridged 3rd ed., Springer, Berlin Heidelberg, 1967 10.1007/978-3-662-06688-1_3.
[15] B. Doudin, M. Viret, Ballistic magnetoresistance? J. Phys.: Condens. Matter 20 (2008) 083201.
[16] Y.V. Sharvin, A possible method for studying Fermi surfaces, Sov. Phys. JETP 21 (1965) 655.
[17] R. Landauer, Spatial variation of currents and fields due to localized scatterers in metallic conduction, IBM J. Res. Dev. 1 (1957) 223–231.
[18] D. Erts, H. Olin, L. Ryen, E. Olsson, A. Thölén, Maxwell and Sharvin conductance in gold point contacts investigated using TEM-STM, Phys. Rev. B 61 (2000) 12725–12727.
[19] R.G. Gatiyatov, V.N. Lisin, A.A. Bukharaev, Ballistic and diffuse electron transport in nanocontacts of magnetics, JETP Lett. 91 (2010) 445–427.
[20] A.B. Pippard, Experimental analysis of the electronic structure of metals, Rep. Prog. Phys. 23 (1960) 176–266.
[21] A.B. Pippard, Magnetoresistance in Metals, Cambridge [England] Cambridge University Press, New York, 1989.
[22] D. Gall, Electron mean free path in elemental metals, J. Appl. Phys. 119 (2016) 085101.
[23] B. Nikolić, P.B. Allen, Electron transport through a circular constriction, Phys. Rev. B 60 (1999) 3963–3969.
[24] E.Y. Tsymbal, I. Zutic, Handbook of Spin Transport and Magnetism, CRC Press, Hoboken, NJ, 2011.
[25] A. Mikrajuddin, F.G. Shi, H.K. Kim, K. Okuyama, Size-dependent electrical constriction resistance for contacts of arbitrary size: from Sharvin to Holm limits, Mater. Sci. Semicond. Process. 2 (1999) 321–327.
[26] G. Eilenberger, Transformation of Gorkov's equation for type II superconductors into transport-like equations, Zeitschrift für Physik A Hadrons and nuclei 214 (1968) 195–213.
[27] J. Rammer, H. Smith, Quantum field-theoretical methods in transport theory of metals, Rev. Mod. Phys. 58 (1986) 323–359.
[28] L.R. Tagirov, B.P. Vodopyanov, K.B. Efetov, Ballistic versus diffusive magnetoresistance of a magnetic point contact, Phys. Rev. B 63 (2001) 104428.
[29] A.N. Useinov, R.G. Deminov, L.R. Tagirov, G. Pan, Giant magnetoresistance in nanoscale ferromagnetic heterocontacts, J. Phys.: Condens. Matter 19 (2007) 196215.
[30] N. Useinov, Semiclassical Green's functions of magnetic point contacts, Theor. Math. Phys. 183 (2015) 705–714.
[31] A. Useinov, J. Kosel, Spin asymmetry calculations of the TMR-V curves in single and double-barrier magnetic tunnel junctions, IEEE Trans. Magn. 47 (2011) 2724–2727.
[32] A. Useinov, Y. Saeed, N. Singh, N. Useinov, U. Schwingenschlögl, Impact of lattice strain on the tunnel magnetoresistance in Fe/insulator/Fe and Fe/insulator/$La_{0.67}Sr_{0.33}MnO_3$ magnetic tunnel junctions, Phys. Rev. B 88 (2013) 060405.
[33] A. Useinov, O. Mryasov, J. Kosel, Output voltage calculations in double barrier magnetic tunnel junctions with asymmetric voltage behavior, J. Magn. Magn. Mater. 324 (2012) 2844–2848.
[34] A. Useinov, L.X. Ye, N. Useinov, T.H. Wu, C.H. Lai, Anomalous tunnel magnetoresistance and spin transfer torque in magnetic tunnel junctions with embedded nanoparticles, Sci. Rep. 5 (2015) 18026.
[35] A. Useinov, H.H. Lin, C.H. Lai, Symmetric and asymmetric magnetic tunnel junctions with embedded nanoparticles: Effects of size distribution and temperature on tunneling magnetoresistance and spin transfer torque, Sci. Rep. 7 (2017) 8357.
[36] N.W. Ashcroft, N.D. Mermin, Solid State Physics, Harcourt Brace College Publishers, New York, 1976.
[37] B.D. Jensen, K. Huang, L.L.W. Chow, K. Kurabayashi, Low-force contact heating and softening using micromechanical switches in diffusive-ballistic electron-transport transition, Appl. Phys. Lett. 86 (2005) 023507.
[38] J.A. Torres, J.I. Pascual, J.J. Sáenz, Theory of conduction through narrow constrictions in a three-dimensional electron gas, Phys. Rev. B 49 (1994) 16581–16584.
[39] D.W. Wong, I. Purnama, G.J. Lim, W.L. Gan, C. Murapaka, W.S. Lewa, Current-induced three-dimensional domain wall propagation in cylindrical NiFe nanowires, J. Appl. Phys. 119 (2016) 153902.
[40] H. Mohammed, H. Corte-León, Y. Ivanov, S. Lopatin, J. Moreno, A. Chuvilin, A. Salimath, A. Manchon, O. Kazakova, J. Kosel, Current controlled magnetization switching in cylindrical nanowires for high-density 3D memory applications, arXiv:1804.06616 (2018).
[41] H. Mohammed, E.V. Vidal, Y.P. Ivanov, J. Kosel, Magnetotransport measurements of domain wall propagation in individual multisegmented cylindrical nanowires, IEEE Trans. Magn. 52 (2016) 1–5.
[42] U. Ebels, A. Radulescu, Y. Henry, L. Piraux, K. Ounadjela, Spin accumulation and domain wall magnetoresistance in 35 nm Co wires, Phys. Rev. Lett. 84 (2000) 983–986.
[43] B.A. Gurney, V.S. Speriosu, J.-P. Nozieres, H. Lefakis, D.R. Wilhoit, O.U. Need, Direct measurement of spin-dependent conduction-electron mean free paths in ferromagnetic metals, Phys. Rev. Lett. 71 (1993) 4023–4026.
[44] G. Pan, Chapter 10 – Thin films for high-density magnetic recording, in: H.S. Nalwa (Ed.), Handbook of Thin Films, Academic Press, Burlington, 2002, pp. 495–553, https://doi.org/10.1016/B978-012512908-4/50075-8 URL: http://www.sciencedirect.com/science/article/pii/B9780125129084500758.

Artur Useinov received a Ph.D. in theoretical physics from Kazan State University (KSU) in 2008 in Russia. He joined King Abdullah University of Science and Technology in Saudi Arabia in 2009 as a Post.Doc. researcher then continued his research in 2013 at California State University, Northridge (W.M. Keck Computational Materials Theory Center). In 2014, he joined National Tsing Hua University (Taiwan) as Research Scientist and further National Chiao Tung University, International College of Semiconductor Technology (Taiwan) in 2017 as Assistant Professor. His research interests include solid-state physics, thin-film heterostructures, quantum and spintronic devices.

Hsiu-Hau Lin received a Ph.D. in physics from the University of California, Santa Barbara in 1998. Then he joined the faculty at National Tsing Hua University since 2000 in Taiwan. He is a theoretical physicist and his research fields include strongly correlated electron systems, low dimensional systems, spintronics, and neurophysics in recent years.

Niazbeck Useinov received a Ph.D. in theoretical and mathematical physics in 1992 from Kazan State University (KSU, Russia). He worked as Assistant and then Associate Professor at Ulyanovsk State University (Russia) until 1999; and since 2003, he is a Chief Scientist and Associate Professor at Kazan Federal University in Russia. He is a theoretical physicist, his research field includes the theory of normal and FM metals, transport properties of mesoscopic systems and spintronics.

Lenar Tagirov received a Ph.D. in theoretical physics in 1981 from Kazan State University (KSU, Russia) and DSc (habilitation) in 1996 from Moscow Engineering Physics Institute (MIFI). Since 1999 he is a Full Professor in the Department of Theoretical Physics in KSU. In 2008 he becomes a head of the Solid Physics Department at Kazan Federal University. In 2016, he joined Zavoisky Physical-Technical Institute of FRC Kazan Scientific Center of RAS in Kazan. Prof. Tagirov is a head of research labs: "Physics of Magnetic Nanostructures and Spintronics" and "Synthesis and Analysis of Thin-Film Structures". He is a member of the Tatarstan Academy of Sciences and an expert in the Russian Academy of Sciences. His research interest includes magnetic nanostructures, magnetoresistance, thin-film heterostructures, tunnel magnetic junctions, superconductivity, superconductor/ferromagnet heterostructures, photonic metamaterials, plasmonic materials, magneto-plasmons.